

PCCP

Accepted Manuscript



This is an *Accepted Manuscript*, which has been through the Royal Society of Chemistry peer review process and has been accepted for publication.

Accepted Manuscripts are published online shortly after acceptance, before technical editing, formatting and proof reading. Using this free service, authors can make their results available to the community, in citable form, before we publish the edited article. We will replace this *Accepted Manuscript* with the edited and formatted *Advance Article* as soon as it is available.

You can find more information about *Accepted Manuscripts* in the [Information for Authors](#).

Please note that technical editing may introduce minor changes to the text and/or graphics, which may alter content. The journal's standard [Terms & Conditions](#) and the [Ethical guidelines](#) still apply. In no event shall the Royal Society of Chemistry be held responsible for any errors or omissions in this *Accepted Manuscript* or any consequences arising from the use of any information it contains.

Intermolecular Network Analysis of the Liquid and Vapor Interfaces of Pentane and Water: Microsolvation Does Not Trend with Interfacial Properties

Yasaman Ghadar, Aurora E. Clark*

¹Department of Chemistry, Washington State University, Pullman, WA 99164

*Authors to whom correspondence should be addressed: auclark@wsu.edu

Abstract:

Liquid:vapor and liquid:liquid interfaces exhibit complex organizational structure and dynamics at the molecular level. In the case of water and organic solvents, the hydrophobicity of the organic, its conformational flexibility, and compressibility, all influence interfacial properties. This work compares the interfacial tension, width, molecular conformations and orientations at the vapor and aqueous liquid interfaces of two solvents, *n*-pentane and neopentane, whose varying molecular shapes can lead to significantly different interfacial behavior. Particular emphasis has been dedicated toward understanding how the hydrogen bond network of water responds to the pentane- relative to the vapor interface and the sensitivity of the network to the individual pentane isomer and system temperature. Interfacial microsolvation of the immiscible solvents has been examined using graph theoretical methods that quantify the structure and dynamics of microsolvated species (both H₂O in C₅H₁₂ and C₅H₁₂ in H₂O). At room temperature, interfacial water at the pentane phase boundary is found to have markedly different organization and dynamics than at the vapor interface (as indicated by the hydrogen bond distributions and hydrogen bond persistence in solution). While the mesoscale interfacial properties (e.g. interfacial tension) are sensitive to the specific pentane isomer, the distribution and persistence of microsolvated species at the interface is nearly identical for both systems, irrespective of temperature (between 273 K and 298 K). This has important implications for understanding how properties defined by the interfacial organization are related to the underlying solvation reactions that drive formation of the phase boundary.

Introduction

The interfacial properties of water with hydrophobic solvents have been an ongoing area of research for many years as these liquid:liquid systems are representative of a broad class of interactions found in biological, chemical, and environmental processes. Alkane solvents in particular are good analogues for developing a general understanding of water hydrocarbon interactions. Early molecular dynamics studies examined the density profiles and molecular orientation at the water:alkane interface, as well as the interfacial tension as a function of organic solvent carbon number, solvent branching, temperature, and force field.¹⁻⁵ Experimental techniques were initially hindered by the small interfacial width of these systems, however over the last 10 years several publications have examined water:alkane interfaces using a variety of experiments that include x-ray and neutron scattering,⁶ optical ellipsometry,⁷ vibrational sum frequency spectroscopy and x-ray reflectivity.^{6, 8-12}

The emergent picture of water:alkane interfaces is complex. Early theoretical studies indicated that water maintains a hydrogen bond network surrounding small microsolvated hydrophobic solutes at an interface, though this network would be stretched with increasing solute size.¹³⁻¹⁵ Stillinger predicted the existence of a depletion layer that is essentially a water:vapor interface that forms near the hydrophobic plane.¹⁵ Numerous experimental studies provided conflicting evidence for and against the presence of a depletion layer,¹⁶⁻¹⁹ but the most recent data has suggested that the attractive van der Waals interactions between a hydrocarbon and water will thin the depletion layer to nearly zero thickness.^{4,6} Microscopic solvation of the macroscopically immiscible solvents can occur, contributing to molecular scale roughening.²⁰ This, in combination with thermally induced capillary wave fluctuations complicates the definition of interfacial width and surface tension.^{21,22}

Microsolvation, interfacial width and tension change with the organic solvent and are believed to play an important role in a myriad of processes including solvent extraction.²³ The variation of interfacial width with carbon number has been described by combining the capillary-wave prediction for the width with a contribution from intrinsic structure. This intrinsic structure is determined by the radius of gyration for the shorter alkanes and by the bulk correlation length for the longer alkanes.⁶ Interfacial properties are also closely linked to the orientational structure of both water and alkane,^{5, 24, 25} as well as the interfacial density, which is related to the solvent compressibility.

Yet our collective understanding of water:alkane interfaces is not definitive and much remains to be studied. For example, little emphasis has been placed upon examining the interfacial hydrogen bond (H-bond) network of water or how this may respond to variations in organic solvent. While significant study has examined how interfacial properties change as a function of alkane chain length,⁴ less emphasis has been placed upon examination of different isomeric forms that may pack differently at the interface. The purpose of the current work is two-fold. First is to understand how the hydrogen bond network of water responds to the presence of the pentane interface and whether the trends in the H-bond network properties coincide with the dependence of the interfacial tension, width, and density upon pentane isomer. Second, we desire to augment these structural properties of the interface with a more detailed description of the interfacial dynamics through the study of microsolvation of the immiscible solvents. It is particularly interesting to examine what, if any, relationship may exist between the mesoscale interfacial properties (e.g. interfacial tension) and the molecular scale dynamics within the typical ns timescale of a simulation. In combination, these data not only help to develop a more holistic understanding of water:alkane interfaces, but they demonstrate the

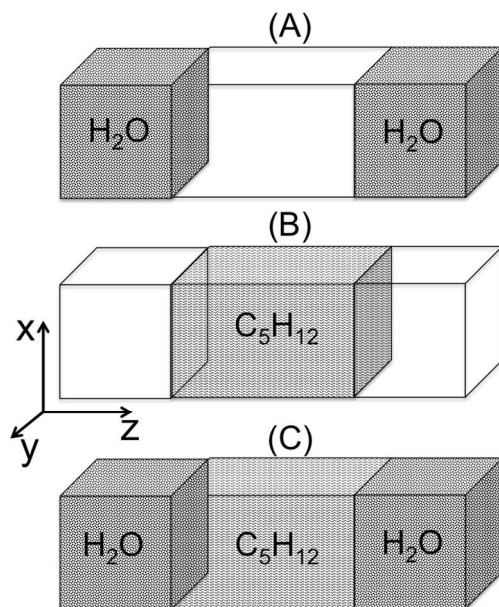
utility of newly developed graph theoretical methods for interrogating interfacial structure and dynamics. The solvents, *n*-pentane and neopentane, have been chosen because they represent two configurational extremes where one isomer is representative of a quintessential chain alkane, while the other is in essence a spherically packing solvent, yet both have the same number of carbons and can utilize the same interatomic potentials for MD simulation. Traditional post-processing analyses are used to investigate the orientational structure of water and *n*-pentane, the interfacial density, as well configurations of *n*-pentane as a function of proximity to the interface. While these analyses support prior observations regarding water:alkane interfaces, the distinguishing feature of this work lies in the application of graph theoretical methods to understand the intermolecular chemical networks in these systems. Analysis of the hydrogen bond network of water, its structure and dynamics, reveals distinctly different behavior between the vapor and pentane interfaces. Intermolecular networks defined by the solvation interactions between water O-atoms and hydrocarbon H-atoms have been used for the first time to quantify microsolvation of the two immiscible solvents. Despite the observation that the interfacial tension and width in the aqueous phase differ significantly between the water:neopentane and water:*n*-pentane systems, the likelihood of microsolvation at the interface and the persistence of microsolvated species are in fact nearly identical. This opens up new avenues for investigating the relationships between the characterizing properties of the interface as a whole, versus the underlying molecular scale processes that drive formation of the phase boundary.

Computational Methods

Molecular Models. Pair-wise additive models represent the potential energy of the system, with intermolecular pair potentials being taken as the sum of all pair potentials between interaction sites within the molecules. The organic molecules *n*-pentane and neopentane have been described by the modified OPLS-AA force field,²⁶ while water utilized a modified rigid TIP3P/Ew water potential.²⁷ All simulations were performed using the LAMMPS software (version 14Feb 2012),²⁸ with the Verlet algorithm and a 1 fs timestep. Ewald summation used a 15 Å cutoff and a 1×10^{-6} tolerance threshold. Tables S1-S2 in *Supplementary Information* present the bonded and non-bonded potentials utilized.

Simulation Details. Five simulation box types were constructed using the Packmol program,²⁹ representing the pentane, water, the pentane:vapor, the water:vapor and the water:pentane systems (Figure 1) using 3-dimensional periodic boundary conditions.

Figure 1. Periodic boundary set-up of (A) the water:vapor, (B) the pentane:vapor, and (C) the water:pentane simulation boxes. Periodic boundaries occur in all three dimensions.



The simulation box of the pure liquids began with an elongated box having $z = 40 \text{ \AA}$ and a cross-sectional area of $30 \text{ \AA} \times 30 \text{ \AA}$; the water simulation contained 1204 molecules, while 376 pentanes were present. Two target temperatures, 273 K and 298 K, were examined as the phase diagram of the neopentane model is not known, and it was desired that the neopentane be a liquid for the neopentane:vapor and water:neopentane simulations. The pure liquids were brought to mechanical and thermal equilibrium at 1 atm using the NVT ensemble of No se and Hoover,³⁰⁻³² followed by a series of NPAT simulations (also known as the effective constant area or the constant pressure, surface area, temperature method), until a pressure of 1 atm was reached. In the NPAT barostat, the volume is varied in only the z -dimension to achieve constant pressure control, which has been shown to help equilibrating systems with nonzero surface tension.³³ The systems were run in NPAT for at least 1 ns followed by 500 ps of simulation in the NVE ensemble to verify the system temperature and pressure.

The liquid:vapor interface simulations had identical x and y dimensions as the pure liquid but with a z -box length such that $\sim 40 \text{ \AA}$ of unoccupied space was left between the two surfaces, while maintaining periodic boundary conditions in all directions (Figure 1). This allowed sufficient space for the liquid and vapor densities to achieve constant values. The simulation boxes were brought to thermal equilibrium using the NVT ensemble with at least 1 ns of simulation and a 1 fs time step. System equilibration was verified during a 500 ps NVE run.

The water:pentane simulations were brought to mechanical and thermal equilibrium at 1 atm by cycling through a combination of the NPAH ensemble and independent Langevin thermostats applied to each phase.³⁴ The NPAH ensemble is similar to the NPAT but without the thermostat. First the system was minimized, then thermostatted for 500 ps in NVT to the

target temperature, thus beginning the cycle of barostatting for 500 ps, relaxing in the NVE ensemble for 500 ps, and repeating until the system was equilibrated. This took at least ten cycles, because a one-dimensional change in the density can induce large changes in the pressure. Production runs for every system consisted of 1 ns of an NVE simulation with capture of the trajectories every 25 fs, leading to a total of 40 K snapshots for data analysis for each ns of the production run. Three 1 ns production runs were performed so as to obtain statistical uncertainties for key interfacial properties. The density profiles, surface tension and interfacial width (defined below) for these interfacial systems were tested for the water:*n*-pentane system using a much larger boxes (in either *x*, *y* or *z*) with dimensions $57 \times 57 \times 157 \text{ \AA}^3$ and $30 \times 30 \times 152 \text{ \AA}^3$ so as to ensure that the data presented in the Results and Discussion is converged with respect to system size.

Data Analysis. The data was analyzed using several methods so as to interrogate the role of the pentane isomer upon interfacial organization and dynamics. Standard analyses included the determination of the radial distribution functions (RDFs) between non-bonded O...O, O...H and the different carbon types present in C₅H₁₅, the radius of gyration (R_g),²⁸ the density profile, as well as the molecular orientation. The orientation order of water is defined as the cosine of the angle θ_i between the unit vector in the direction of the dipole (μ_i) and the unit vector normal to the interface (n_z),

$$\cos\theta_i = \mu_i \cdot n_z, \quad (1)$$

while the *n*-pentane orientation is defined as

$$S_z = \frac{1}{2}(3 \langle \cos^2\theta \rangle - 1) \quad (2)$$

Here θ is the angle between the molecular axis and the interface normal (*z*-axis), where the brackets imply averaging over time and molecules. The molecular axis is defined as the vector

from C_{n-1} to C_{n+1} and thus there are three vectors for n -pentane. The order parameter can vary between 1 (full order along the interface normal) and $-1/2$ (full order perpendicular to the normal), with a value of zero in the case of an isotropic orientation (Figure S1 in *Supplementary Information*).⁴

The interfacial tension (γ) was calculated in two ways. The first method is based upon measurement of the pressure tensors in each dimension:

$$\gamma_P = \frac{1}{2} L_z [\langle P_{zz} \rangle - \frac{1}{2} (\langle P_{xx} \rangle + \langle P_{yy} \rangle)] \quad (3)$$

where P_{zz} is the normal pressure, and P_{xx} and P_{yy} are the tangential pressures with respect to the planar interface. However this approach assumes a sharp liquid:vapor interface, when in reality it is quite rough because the interface breaks the translational invariance of the system, inducing experimentally observed Goldstone fluctuations or “capillary waves”.^{21, 22, 35, 36} Thus a second method was used for computing the surface tension that takes into account fluctuations from an intrinsic contribution plus a logarithmic term that represents the broadening of the interface.^{33, 37-}

³⁹ The total interface profile $\Psi(z)$ may be expressed as a convolution of the intrinsic profile $\psi(z)$ and the effect due to capillary waves.

$$\Psi(z) = \int_{-\infty}^{\infty} \psi(z - z_0) P(z_0) dz_0 \quad (4)$$

where, $P(z_0)$ is the probability of finding the interface at z_0 .

Decoupling the capillary wave and the density fluctuation contributions makes it possible to compute the surface tension from the interfacial profile (or scaled density profile) along z . The interfacial profile has a density range from 1 to -1 and has the form:²¹

$$\Psi(z) = \frac{2}{\rho_l - \rho_v} (\rho(z) - \frac{\rho_l + \rho_v}{2}) \quad (5)$$

where $\rho(z)$ is the density in the z -direction, while ρ_l is the liquid density and ρ_v is the vapor

density. Given $\Psi(z)$, the variance of the profile, $\frac{d\Psi(z)}{dz} = \Psi'(z) = f(z)$, can be used as a measure of the width of the interface.²² The variance of a distribution f is given by

$$v(f) = \frac{\int_{-\infty}^{\infty} z^2 f(z) dz}{\int_{-\infty}^{\infty} f(z) dz} = \frac{-\frac{d^2}{dq^2} \tilde{f}(q)|_{q=0}}{\tilde{f}(0)} \quad (6)$$

where $\tilde{f}(q)$ is the Fourier transform of $f(z)$. Using the convolution theorem and Eqns. (5) and (6) it can be shown:²¹

$$v[\Psi'] = v[\psi'] + v[P] \quad (7)$$

The squared widths of the total and intrinsic interfacial profiles have been defined as $\Delta^2 \equiv v[\Psi']$ and $\Delta_0^2 \equiv v[\psi']$, respectively. The average squared fluctuations of the interface about its mean location in the z -direction can be directly identified as $v[P]$.²¹ Since the mathematical form of the variance is cumbersome to evaluate, the scaled interfacial profile is typically fit to a hyperbolic tangent function as in Eqn. (8),^{38, 40} however more recent work has indicated that the error function often yields results closer to experiment, as in Eqn. (9):²²

$$\Psi_t(z) = \tanh\left(2\left(\frac{z-z_0}{w_t}\right)\right) \quad (8)$$

and

$$\Psi_e(z) = \text{erf}\left(\sqrt{\pi}\left(\frac{z-z_0}{w_e}\right)\right) \quad (9)$$

In the liquid:vapor systems the interfacial thickness has been determined by fitting both Eqn. (8) and (9) which includes determining the average location of the Gibbs dividing surface, z_0 , within $\rho(z)$. The position of the Gibbs dividing surface has been defined as $\rho(z) = \frac{(\rho_l + \rho_v)}{2}$ and is presented in Table S3 in *Supplementary Information* for all systems under consideration.

Depending on whether Eqn. (8) or Eqn. (9) are used, two definitions of the interfacial width emerge:

$$\Delta^2 = \begin{cases} \frac{w_e^2}{2\pi} & \text{if fit to Eq. 8} \\ \frac{\pi^2 w_t^2}{48} & \text{if fit to Eq. 9} \end{cases} \quad (10)$$

The surface tension is obtained by plotting the interfacial width, Δ , obtained from different values of the Gibbs dividing surface, z_0 . This, in essence, means that the profile is fit at different depths within the box (near the interface and sequentially deeper in the bulk). The interfacial tension is derived from the best fit line of Δ^2 vs. $\ln(L)$ as, $\gamma_w = k_B T / (2\pi \text{ slope})$,⁴¹ where L is the length of the simulation box in the z -direction.

To calculate the surface tension from the capillary wave method, the procedure of Senapati and Berkowiz was followed,⁴⁰ where the density profile of water (ρ_w) and alkane (ρ_a) is fitted to Eqn. (11) and Eqn. (12) respectively:

$$\rho_w(z) = 0.5\rho_w - 0.5\rho_w \operatorname{erf}\left(\frac{z - z_{0,w}}{\sqrt{2}w_c}\right) \quad (11)$$

$$\rho_a(z) = 0.5\rho_a - 0.5\rho_a \operatorname{erf}\left(\frac{z - z_{0,a}}{\sqrt{2}w_c}\right) \quad (12)$$

In equations 11-12, $z_{0,w}$ and $z_{0,a}$ represent the Gibbs dividing surface for water or alkane, respectively. The width due to thermal fluctuations is w_c while the intrinsic width w_0 is $|z_{0,w} - z_{0,a}|$ and the total width is w . The three terms are related by: $w^2 = w_c^2 + w_0^2$. After finding the value of w_c , one can find the value of γ_e due to the capillary wave and thermal fluctuations using Eqn. (13):⁴²

$$w_c^2 = \frac{k_B T}{2\pi\gamma_e} \ln\left(\frac{L_x}{l_b}\right) \quad (13)$$

where L_x is the total length in the $x=y$ direction and l_b is the bulk correlation length (on the order of the molecular length). In this work we have estimated the value of l_b as the cut off distance of 15 Å.⁴⁰

Topological Analysis of the Hydrogen Bond Network. The essential properties of the hydrogen bond network of water have been analyzed using a graph theoretical approach implemented in the *ChemNetworks* software package,⁴³ available for download at <http://aclark.chem.wsu.edu/software/>. Each snapshot is converted into a graph wherein the H₂O molecules are vertices and an edge is created between vertices by the presence of an intermolecular hydrogen bond. In this work, a geometric criterion within a distance threshold between the non-bonded O- and H-atoms of $r < 2.5$ Å and a H-bond angle of 150-180°, was utilized (Figure S2 in *Supplementary Information*). This yields a distribution of hydrogen bonds for each molecule whose weighted average is approximately the same as the total average number of H-bonds as indicated by the RDF. Thus, one of main strengths of the network analysis is that it easily decomposes the information that would be in an RDF into its component contributions. While the RDF yields the average H-bond environment about a given water, the network analysis provides the relative % of waters with 1 – 4 H-bonds that yield that overall H-bond number. Topological analyses of the graph were performed for different layers as a function of distance from the vapor and pentane interfaces, respectively. First, the histogram of the distribution of H-bonds was obtained in a 12 Å layer from the Gibbs dividing surface. This yields information about how the average local hydrogen bond environment changes during the transition from the interfacial region to the bulk. The persistence of the hydrogen bonds was also obtained, yet accurate statistics required use of much larger layers that essentially split the water portion of the simulation box into two halves. The persistence is the weighted average number

of fs that a H-bond edge is observed for all edges considered. Persistence is different from the “lifetime” of the H-bond because transient breaks in the time of the existence of the edge are included in the calculation. Despite the large size of the layers within this calculation, statistically different persistence values for the H-bonds in those regions were obtained. Persistence is a useful construct to understand the mechanisms behind H-bond formation and breakage events because it does not discount short time-scale behavior. To further probe these dynamics, each instance of edge deletion/formation was cross-correlated to the distance travelled by the respective water molecule vertices in between snapshots, thus probing whether diffusion causes H-bond breakage. Librational motion may also alter H-bond patterns and thus the dynamic behavior of the dipole orientation of solvating water about reference water molecules was investigated. The orientation of the dipole moment vector of a water molecule, \mathbf{P} , with respect to a reference molecule to which it is H-bonded, referred to as the “dipole angle” is defined in Figure S3 in *Supplementary Information*. To investigate whether the dipole orientation dynamics is altered as a function of distance from the interface, a series of water molecules were chosen as “reference” molecules. The dipole orientation of the solvating waters about the reference molecules were then tracked over time as the reference molecules moved from the interfacial region to the bulk.

Potential of Mean Force and Microsolvation. Several prior studies have noted the importance of microsolvation (the solvation of one solvent by another at the molecular level) at liquid:liquid interfaces.^{21, 38, 44} At water:oil interfaces in particular, water penetration on the molecular scale is believed to be a common phenomena.⁴⁵ We have previously investigated this via quantum mechanical calculations of solvated clusters of water about neopentane and *n*-pentane (and *vice versa*), wherein we examined the thermodynamic favorability of

microsolvation.⁴⁶ In the classical analogues, potential of mean force calculations are a useful complement to the quantum mechanical study by investigating the energetic and structural features associated with water penetration into pentane and pentane into water. An umbrella-sampling scheme was used to calculate the unbiased free energy $A(\xi)$ along the reaction coordinate.⁴⁷⁻⁴⁹ Umbrella sampled windows were then combined with the umbrella integration method.⁴⁸⁻⁵⁰ The reaction coordinate involved dragging a single molecule from the center of its liquid phase to either the liquid:vapor interface or migration through the interface and to the center of the second solvent box. A harmonic biasing potential was used with a force constant of $0.5 \text{ kcal/mol}\text{\AA}^2$ to drag a molecule within 0.5 \AA intervals and 0.5 ns simulation time. The width of each bin within the umbrella integration was set to 0.03 \AA .

The PMF simulations yield thermodynamic information, however the kinetic aspects of phase penetration are better understood by the explicit determination of microsolvated clusters within the interfacial regions of the water:pentane systems. To do this, water molecules and pentane molecules were converted to vertices and an edge defining their solvation interaction was formed if the distance between the water O-atoms and the pentane H-atoms $r_{\text{O..HC}}$ is $< 4.3 \text{ \AA}$. This distance was chosen based upon the previously determined two-body CCSD(T) potential energy surfaces reported in reference 46. The resulting distributions describe the percent observation of pentane molecules non-solvated, partially- or fully solvated by water and *vice versa*. The persistence of each microsolvated cluster was also determined.

Results and Discussion

The results first consider the pure liquid systems, then the liquid:vapor and water:pentane systems as a function of pentane isomer. Finally the potential of mean force data

for the water:pentane systems is presented along with the microsolvation analysis. Special effort is dedicated to the comparison and contrast of the water orientation, dynamics, and hydrogen bond patterns in the three interfacial systems so as to understand how water not only responds to the hydrophobic solvent, but also to pentane packing and other metrics of interfacial structure.

Pure Liquids. Much work has been performed regarding the physical properties and dynamics of neopentane, *n*-pentane, and TIP3P/Ew water. The simulations here reproduce the radial distribution functions, densities, and diffusion coefficients of the pure liquid phases at several temperatures^{27, 51-55} (Table S4 and Figures S4-S6 in *Supplementary Information*). In comparison to the liquid:vapor and liquid:liquid interfacial systems a few key structural and dynamic pieces of information are relevant.

The histogram of the hydrogen bond distribution for TIP3P/Ew water is presented in Figure 2 at 298 K and 273 K. The H-bond distribution of this water model at room temperature is quite similar to that of Amoeba water, which has been previously discussed.⁴³ Namely, 36% of waters have 4 H-bonds, while 39% have 3 H-bonds, 18% have 2 H-bonds, 4% have 1 H-bonds and a small percentage of molecules with zero or five H-bonds. Taking the weighted average of these values yields 3.13 H-bonds per water molecule, which is in a good agreement with the RDF between the non-bonded O...H atoms (Figure S4 in *Supplementary Information*). As the temperature is cooled to 273 K, the expected increase in concentration of 4-coordinate H-bonded waters is observed as the hydrogen bond network has less thermal fluctuations and the weighted average increases to 3.35 H-bonds per H₂O. At 298 K the average H-bond persistence is 170 ± 2 fs, while this increases to 216 ± 4 fs at 273 K (Table 1). This is in a good agreement of previous studies of the persistence of the H-bond of 180 fs and 230 fs at 300 K and 275 K, respectively, using a similar geometric definition.⁵⁶

Figure 2. Hydrogen bond distribution for bulk and interfacial water in the liquid:vapor systems at 298 K and 273 K. The average number of H-bonds per H₂O molecule is given as $\langle n_{\text{HB}} \rangle$.

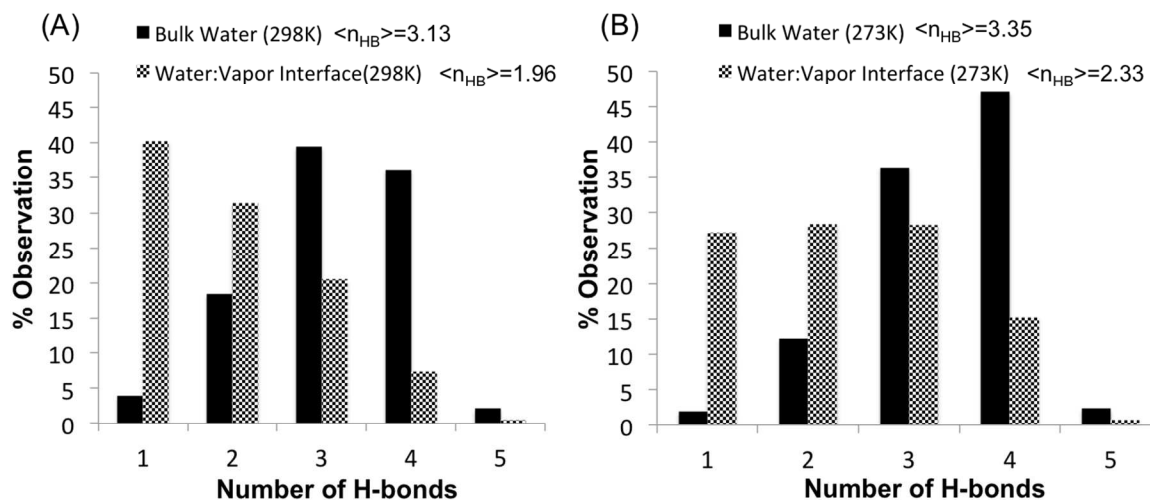


Table 1. Average H₂O...H₂O H-bond persistence (P) in fs, for bulk water at 298 K and 273 K, and H₂O in the vapor and pentane interfacial regions (defined as the center-of-mass existing within 12 Å of the Gibbs dividing surface, see Table S3 in *Supplementary Information*).

T	P (Bulk)	P (at Vapor Interface)	P (at Pentane Interface)
273 K	216±4	135 ±1	129±4 (with neopentane)
298 K	170 ±2	111±1	134 ±1 (with <i>n</i> -pentane)

In the pure pentane liquids, the RDF between the non-bonded central C-atoms of neopentane indicates a primary solvation shell at a central C-atom distance of ~ 6 Å, containing 10-12 molecules (Figure S5-S6 in *Supplementary Information*). The peak in the RDF is quite broad, indicating a lack of organizational structure. In contrast to neopentane, *n*-pentane has both terminal methyl as well as central C-atom types. This makes interpretation of the RDFs difficult, particularly when combined with the observation that *n*-pentane can adopt multiple configurations in solution. The radius of gyration, R_g , is one metric for assessment of the conformations of *n*-pentane in solution. Yet a major drawback is that R_g does not track linearly with changes in the dihedral angles of *n*-pentane and thus it cannot be easily correlated to a

systematic rotation in angle that corresponds to transformations between minima on the dihedral angle potential energy surface. Here, R_g is used as a metric for relative populations of different conformations observed in solution, not for the identification of those conformations. This is most relevant when considering the changes in the orientational order, S_z , of *n*-pentane at the vapor and aqueous interface (*vide infra*). As presented in Table 2, *n*-pentane molecules dynamically change configurations over time, however the most commonly observed configurations as identified by their R_g values are conformations 2 and 4 which are observed 7-9% of the time followed by conformations 3, and 5 which are observed ~5% of the time.

Table 2. Radius of gyration, R_g , values of *n*-pentane and their % observation in the bulk and at the vapor and aqueous interfaces (defined as being within 12 Å of the Gibbs dividing surface, see Table S3 in *Supplementary Information*).

R_g	Conformation ID	% in Bulk	% at Vapor Interface	% at H ₂ O Interface
1.939-1.934	1	2.47		
1.924-1.914	2	7.95	20.24	19.14
1.914-1.909	3	5.48	12.04	11.53
1.909-1.899	4	9.32	17.52	17.53
1.899-1.894	5	4.11		
1.894-1.889	6	3.29		

Liquid:Vapor Interfaces. Traditional analyses of the simulation data of liquid:vapor interfaces have focused upon understanding the interfacial molecular orientation as well as the surface tension and width. The density profile of the water:vapor boxes at 273 K and 298 K agree with previous studies (Figure S7 in *Supplementary Information*) and the dipole orientational profile supports prior observation of a bimodal distribution for interfacial water (Figure 3). Specifically, the layer of water closest to the interface (H₂O whose center-of-mass, COM, is within 8 Å of the vapor phase, e.g. $z = 33 - 38$ Å at 273K) adopts an orientation wherein the water dipole lies in the plane of the interface, followed by a second layer farther

from the interface (between 8 and 13 Å of the vapor phase) that adopts an orientation with the H₂O dipole directed out of the liquid at an angle of 74° relative to the surface normal.

In addition to altered orientations, those waters within 12 Å from the Gibbs dividing surface (see Table S3 in *Supplementary Information*) also have a perturbed distribution of hydrogen bonds relative to the bulk. In general there is a decrease in the concentration of H₂O with three and four H-bonds and an increase in those with one and two H-bonds. As seen in Figures 2A and 2B, there are distinctly different H-bond distributions for these interfacial water at 298 K and 273 K. At room temperature, nearly 40% of interfacial H₂O have a single H-bond (or exist as a H-bonded dimer), with ~30% having two H-bonds (statistical variances presented in Table S5). In contrast, at 273 K, there are many more interfacial waters (within 12 Å from the Gibbs dividing surface) with three H-bonds, and the concentration of H₂O with 1 – 3 H-bonds is nearly equal. Variations in the H-bond distribution are to be anticipated within the 12 Å definition of the Gibbs dividing surface, with the H₂O directly in the transition to the vapor phase having the least number of H-bonds. The average hydrogen bond persistence for water in this region is also shorter than in the bulk at the two temperatures examined. At 298 K interfacial waters have an H-bond persistence of 111 fs, while at 273 K interfacial waters have a longer persistence value of 135 fs (Table 1). Relative to the bulk values at the two temperatures, this represents a statistically significant decrease in H-bond persistence for those waters in the interfacial region of 8-10%. This approach supports prior observations⁵⁶ that have used a geometric criterion of an H-bond followed by examination of the decay rate of an initial set of H-bonds in the liquid simulation in addition to H-bond lifetimes approximated by the orientational relaxation times of interfacial waters within water-ammonia mixtures.⁵⁷

Figure 3. (A) Dipole angle orientation of water in the water:vapor system at 298 K and 273 K, as compared to water:neopentane (273 K) and water:*n*-pentane (298 K). (B) The *n*-pentane order parameter in *n*-pentane:vapor and water:*n*-pentane at 298 K. A relative *z*-axis (z_{rel}) has been used so as to overlap the spectra for optimal comparisons of behavior.

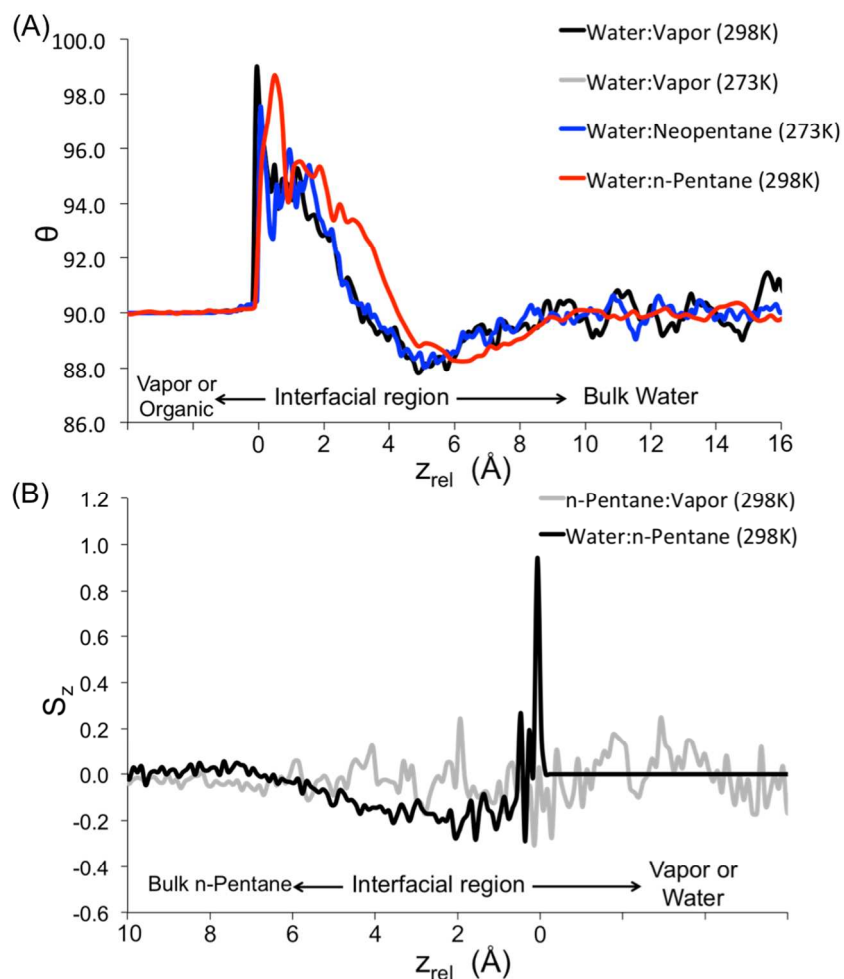
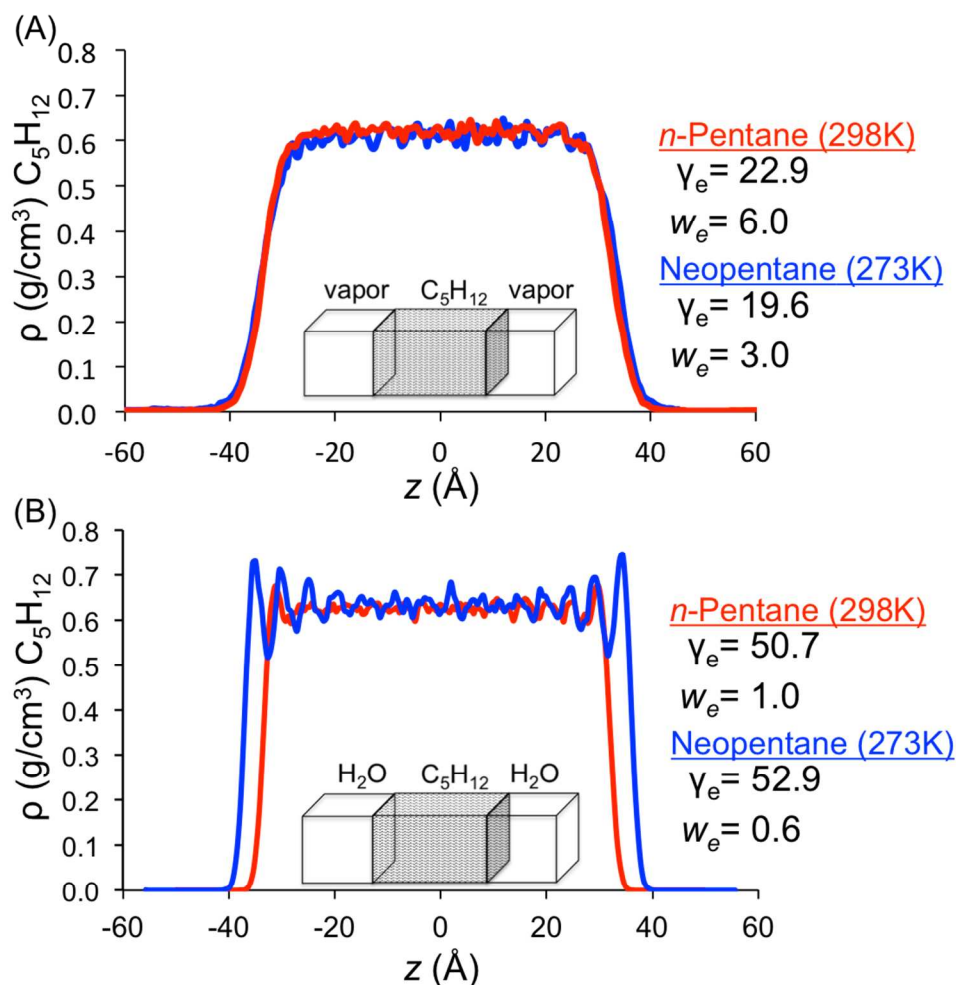


Figure 4. Density profiles of (A) pentane:vapor and (B) water:pentane at 298 K and 273 K (for the sake of clarity the water density profile is shown in Figure S8 in the *Supplementary Information*).



The decrease in the H-bond lifetime at the vapor interface may be caused by several factors. First, it has been previously reported that the self-diffusion constant of water may be up to 67% larger at the interface than in the bulk.^{58, 35} Alternatively, changes in the rotational dynamics may alter the H-bond persistence through librational motion.⁵⁹⁻⁶¹ To further probe the mechanisms of the hydrogen bond breakage and formation at the bulk vs. the interface, two different analyses have been performed. First, each instance of H-bond formation and deletion

has been cross-correlated with the change in Euclidean distance of the O-atoms of the water atoms involved in the H-bond. It is readily apparent that nearly all H-bond breakage and formation reactions are not the result of diffusion because $\Delta r_{O\dots O}$ is much less than the diffusion coefficient would predict using a 25 fs timestep in between frames (Table S5 in *Supplementary Information*).⁶² The second analysis has involved study of the dipole moment orientation of solvating water about a reference H₂O at the interface and as it diffuses into the bulk region over time. Within the current implementation of *ChemNetworks* the dipole angle analysis is not automated and thus the dipole angles of solvating molecules about 2-4 reference molecules were examined at each temperature. Within this limited set of reference molecules no statistically different dynamics in the angle oscillations could be discerned. Thus no satisfactory explanation of the decrease in H-bond persistence in the interfacial region has been obtained at this time. This is, however, a topic of ongoing study, as very good statistics may be needed to obtain any correlation between changes in librational dynamics and H-bond persistence.

In summary, these data indicate that the H-bond network of water near the vapor interface is significantly perturbed relative to the bulk and that this perturbation alters both the distribution of hydrogen bonds at the interface as well as the H-bond persistence. In order to get good statistics, these analyses utilized a very broad definition of the “interfacial region” in the water:vapor simulation (within 12 Å from the Gibbs dividing surface), however both the size of the interfacial region and the surface tension can be mathematically determined using either the capillary wave or pressure tensor methods described in Equations (3), (8) and (9). Prior MD simulations have indicated that the water:vapor interface is not sharp at a microscopic level and has a thickness of 3.2 Å at 298 K.⁶³ The calculated surface tension and interfacial width values presented here for TIP3P/Ew at 298K are in good agreement with prior theoretical studies using

TIP4P and SPC potentials (Table 3). However those works have indicated that most of water models underestimate the surface tension (γ) from its experimental values by 25-50%.^{22,64} Indeed, as observed in Table 3, at 298 K, the surface tension obtained from measurement of the pressure tensors is 36% lower than experimental values, while that obtained from fitting the interfacial profile to an error function is 38% lower (hyperbolic tangent fits presented in Table S7 in *Supplementary Information*). The anticipated increase in the surface tension occurs upon cooling to 273 K by 30%,²² while at the same time the interfacial width decreases (note that the TIP3P/Ew model does not freeze until 146 K⁶⁵). Previous x-ray reflectivity measurements of water at 298 K have reported surface roughness or interfacial thickness of 1.8 Å which is 0.5 Å longer than the calculated value of 1.2 Å (Table 3).²⁰

Table 3. Surface tension values γ_p and γ_e . The quantity γ_p was evaluated using Eqn. (3), while γ_e is based on capillary wave method and was determined using Eqn. (9). The interfacial thickness parameter, w_e , and interfacial width, Δ_e , of liquid:vapor and w_0 of liquid:liquid interfaces are also presented.

Interface T(K)	γ_p (dyne/cm)	γ_e (dyne/cm)	w_e (Å)	Δ_e or w_0 (Å)
Water:Vapor@ 298	49.6(51.6 ⁶⁴ , 47.4 ⁶⁶)	44.3	3.1	1.2(1.8 ²⁰)
Water:Vapor@ 273	64.8(54.6 ⁶⁴)	63.2	2.8	1.1
<i>n</i> -Pentane:Vapor @ 298	16.6(15.9 ⁶⁷ , 15.3 ⁶⁸ , 15.5 ⁶⁹ 17.9 ⁷⁰)	22.9	6.0(6.2, 9.5 ²)	2.4
Neopentane:Vapor@ 273	20.4	19.6	3.0	1.2
Water: <i>n</i> -Pentane@298	51.4(50.9 ⁷¹ , 50.8 ²)	50.7	1.0(1.1 ²)	0.6(0.8 ²)
Water:Neopentane@298	38.6	41.6	1.2	1.1
Water: <i>n</i> -Pentane@273	51.2	48.6	1.1	1.1
Water:Neopentane@273	47.8	52.9	0.6	1.7

As shown in the density profile (Figure 4A), the vapor interfaces of both neopentane and *n*-pentane exhibit the same density and thus there is no significant packing difference for the two isomers. Recall that two different temperatures are used for the *n*-pentane:vapor and neopentane:vapor interfaces due to the high vapor pressure of neopentane at 298K using this force field. Yet, other measures of interfacial structure indicate significantly different interfacial

properties that could be related to the differences in compactness of the pentane isomer. At 298 K, *n*-pentane is found to have a thickness order parameter of 6.0 Å, which decreases to 3.0 Å for the neopentane:vapor interface at 273 K. Since the interfacial density is the same for both neopentane and *n*-pentane, this may be due to the decreased temperature used to simulate the neopentane:vapor system, however similar behavior is observed in the water:neopentane simulations where the same temperatures were able to be studied for both *n*-pentane and neopentane. Prior studies using the maximum bubble pressure method for the *n*-pentane:vapor interfacial tension have reported a value of 15.3 dyne/cm at 298 K and 1 atm,⁶⁸ which is in good agreement with the predicted value of 16.6 dyne/cm obtained using Eqn. (3). Consistent with the decreased interfacial width for the neopentane:vapor interface at 273 K is a larger predicted interfacial tension of 20.4 dyne/cm. The capillary wave (γ_e) approach for determining interfacial tension results in somewhat larger values of 19.6 and 22.9 dyn/cm for *n*-pentane:vapor and neopentane:vapor, respectively. These data agree with the general observation that a decreased surface tension usually is accompanied by an increased interfacial width.^{22, 40} Both approaches for determining the surface tension of the pentane:vapor systems predict an increase in the surface tension for the more compact neopentane isomer relative to the chain *n*-pentane isomer, however prior work has shown that both a decrease in the temperature as well as the size of a molecule may be responsible for this result.^{66, 72} In the water:neopentane systems, the vapor pressure of the neopentane is not an issue, and thus direct comparisons have been made between the interfacial properties of water:neopentane and water:*n*-pentane at the same temperature.

Figure 5 presents the order parameter S_z of *n*-pentane in the *n*-pentane:vapor system with respect to the *z*-axis. It is clear that during the transition into the interfacial region (defined by

Gibbs dividing surface at $z = 33 \text{ \AA}$), the molecular orientations/conformations become less isotropic, indicating a small amount of orientational dependence at the interface. As indicated by Figure S1, an S_z value of ± 0.05 to ± 0.10 correlates to an average angle of the three vectors of *n*-pentane between $40\text{-}60^\circ$. Since S_z is altered by both the conformation that *n*-pentane adopts as well as the overall orientation of the molecule relative to the interfacial plane, it is important to attempt to deconvolute these two contributing factors. Examination of R_g to analyze the *n*-pentane conformations indicates that there is a decrease in the conformational space adopted in the interfacial region with the vapor phase. Here, the center of mass (COM) was used to assign *n*-pentane molecules to the interfacial region, which starts at $z = 33 \text{ \AA}$ in the density profile in Figure 4. As seen in Table 2 it is apparent that the bulk *n*-pentane molecules have a broad range of conformations that are observed individually only 5-10% of the time, however at the edge of the vapor interface up to 20% of the interfacial molecules adopt conformations 2, 3 and 4 as the *n*-pentane molecules escape the liquid phase. Though these observations expand upon previous reports that had concluded that conformational variation expands as alkanes escape into the gas-phase,⁷³ it is important to note that different criteria may yield altered interpretations of the interfacial ordering, as discussed in ref. 74 for acetonitrile interfaces.⁷⁴

Water:Pentane Interfaces. Highly immiscible liquid:liquid phase boundaries are typically characterized by an extremely narrow interfacial region with a high interfacial tension. The net orientations of the alkanes in the interfacial region are generally found to lie perpendicular to the plane of the interface.⁵ Water on the opposite side of the interface orients to maximize hydrogen bonding,⁵ though to what extent the hydrogen bonding is modified has not been examined. Further, the interfacial tension typically decreases as the number of carbons increase in the organic solvent in water:alkane systems.^{71, 75} In this work, analysis of

water:neopentane density profiles demonstrates an $\sim 10\%$ increase in the interfacial density of neopentane relative to *n*-pentane (Figure 4). Though the density oscillates at the interface for both pentane isomers, the oscillation significantly increases in subsequent layers of neopentane moving from the interface into the bulk, as previously observed in water:carbon-tetrachloride systems.⁷⁶ Since this phenomena is not observed in the pentane:vapor systems at the same temperature, it appears that the hydrophobic interaction and presence of the aqueous phase is responsible for the altered solvent packing of pentane in the interfacial region.

Analysis of the interfacial tension and interfacial thickness also reveal important deviations in the interfacial properties as a function of the isomeric form of pentane. As presented in Table 3 the interfacial tension calculated for water:*n*-pentane are in excellent agreement with previous studies.^{2, 71} At 298 K, neopentane is predicted to have a 17% smaller surface tension and 45% larger interfacial width relative to *n*-pentane (using Eqn. 9-10). This might be expected from the general observation that a decrease in alkane chain number decreases the interfacial tension in aqueous:organic systems. Interestingly, as the temperature is decreased to 273 K, the dependence of the interfacial properties upon isomer form becomes less straightforward. Similar surface tensions are observed for both water:neopentane and water:*n*-pentane, yet the interfacial width is predicted to be larger for neopentane, in disagreement with the measured increase in the interfacial thickness parameter. The orientational order parameter of *n*-pentane supports a perpendicular orientation relative to the interfacial plane, however the distribution of R_g values of *n*-pentane near the interface (defined by the Gibbs dividing surface) is very similar to that observed at the vapor interface (Table 2).⁴ Thus, the presence of water at the interface clearly orients the pentane, as opposed to changing the conformations populated in the interfacial region. As water has an impact upon the *n*-pentane orientation, the organic solvent can also effect the

angles that water forms with respect to the normal of interface. While water in the closest layers to the interface exhibits a bimodal angular distribution in all systems, the water molecules deep in the interfacial region ($z = 32 - 42 \text{ \AA}$ in Figure 4A) exhibit more orientational ordering in the water:*n*-pentane system than in neopentane (Figure 3).

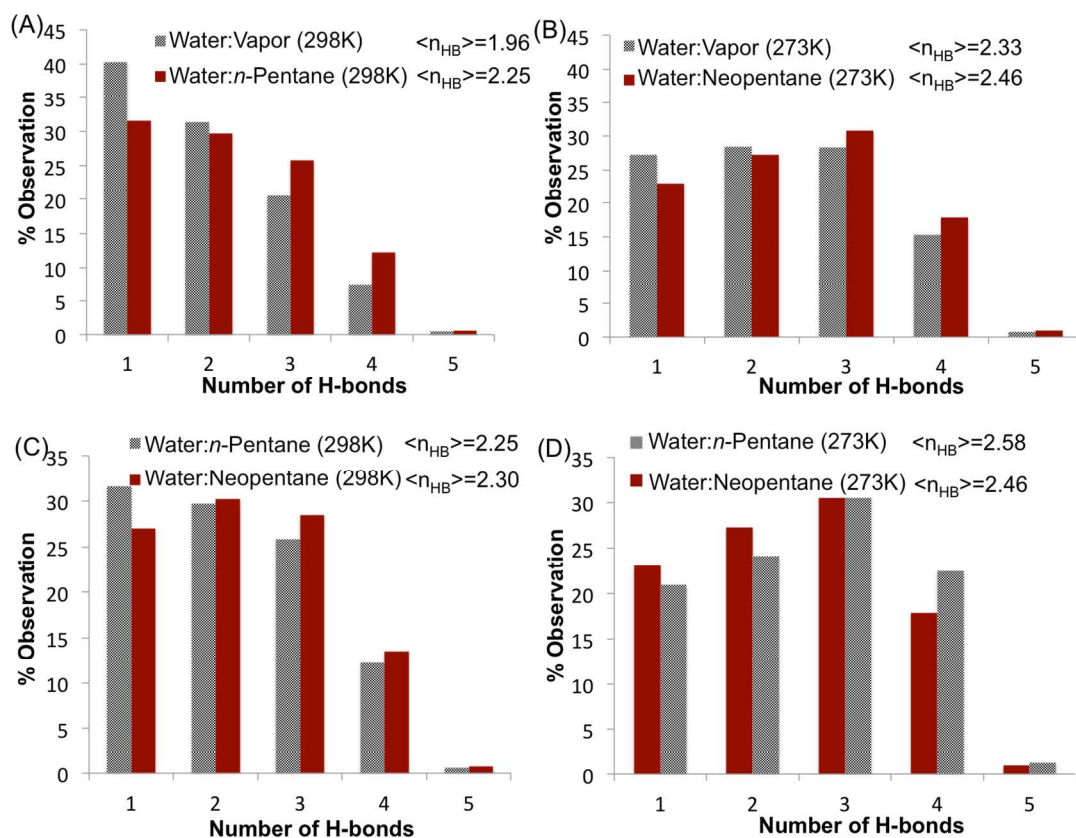
Analysis of the H-bond distributions of water within 12 \AA from the Gibbs dividing surface provides further insight into the response of water to the presence of the pentane solvent. As observed in Figure 7, waters in this region of have a higher average number of H-bonds than at the analogous vapor interface at the same temperature. Water near *n*-pentane and neopentane at 298 K display a 5-10% increase in population of molecules with three and four H-bonds, while the same trend is observed at 273 K but to a smaller extent because bulk water at 273 K generally has a larger concentration of higher coordinate waters (Figure 2). This complements the water dipole orientation data presented in Figure 3, wherein the orientational structure of water in water:*n*-pentane extends deeper from the interfacial to bulk regions relative to all other systems. Interestingly, the interfacial H-bond distributions in the water:vapor systems exhibit a larger sensitivity to the temperature than interfacial water near the pentane interfaces. This may be due to a dampening in the thermally induced fluctuations (librational motion) in the presence of a liquid interface, or because less interfacial water molecules are actively leaving the aqueous phase to be microsolvated in the pentane vs. escaping into the vapor (*vide infra*). The H-bond persistence within 12 \AA from the Gibbs dividing surface of the pentane interface complements the changes observed in the hydrogen bond distribution, wherein interfacial water still exhibit shortened H-bond persistence relative to the bulk (Table 1). However, the H-bond persistence of interfacial water at 298 K with either *n*-pentane or neopentane is longer than interfacial water:vapor, presumably due to the higher concentration of more highly coordinated waters in

the water:pentane systems. The difference between the H-bond persistence at 273 K for the water:vapor and water:pentane systems is less pronounced and almost within the statistical error of the two calculations, as would be anticipated based upon the similarity in the distribution of H-bonds in the two systems. In combination, these data clearly indicate that interfacial water near the pentane interface differs significantly from interfacial water near a vapor interface (particularly at room temperature).

In order to understand whether water responds differently to the two isomers of pentane, the H-bond distributions for water within 12 Å from the Gibbs dividing surface of the neopentane and *n*-pentane interfaces were examined. As observed in Figure 7, the H-bond distributions of water are very similar but statistically different from one another (Table S8 in *Supplementary Information*). At room temperature, water has a slightly higher average number of H-bonds when in the presence of neopentane, while at 273 K water is slightly more organized near the *n*-pentane interface. This trend is opposite that observed at the water:vapor interfaces at 298 K and 273 K, where an increase in surface tension coincided with an increase in the number of interfacial water molecules with exactly four H-bonds. In general, these data indicate a limited ability of water to differentiate between the two isomers of pentane at a fixed temperature within this region from the interface. It may be that H₂O directly interacting with the two pentane isomers may exhibit varied properties, however the data obtained regarding the microsolvated species at the interface (*vide infra*) does not support this. Given that the presence of the pentane clearly alters the hydrogen bond network of water relative to the vapor phase, current work within our group is pursuing what extent of difference in solvent shape and electrostatic properties is necessary to induce a significant response in the interfacial water organization at an interface with an organic solvent. Further, since the hydrogen bond network of water is much

less sensitive to the pentane isomer than the mesoscopic interfacial properties like interfacial tension, is unclear what, if any, correlation these properties have with the molecular-scale dynamic features of the interface.

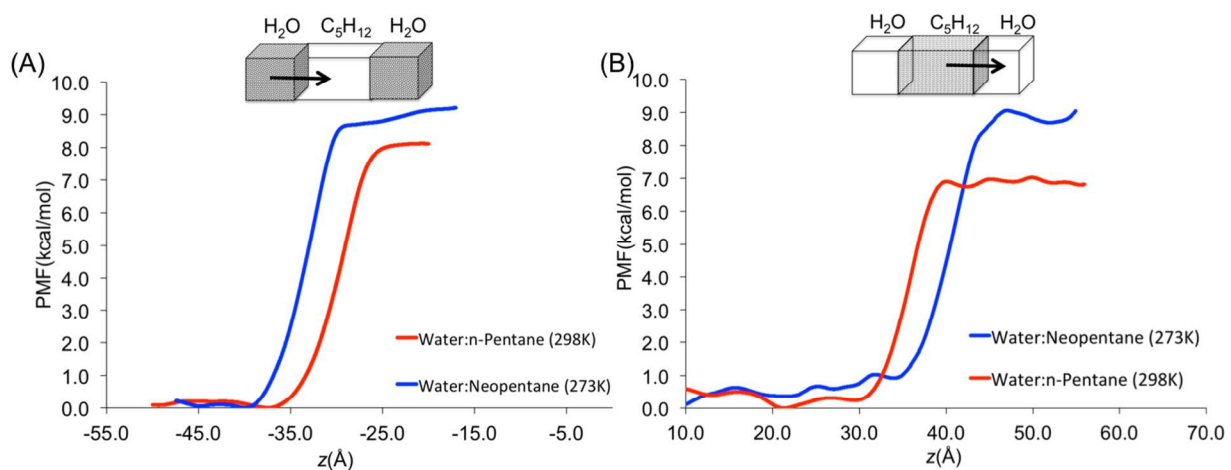
Figure 7. Hydrogen bond distribution for the interfacial section of liquid:vapor and water:pentane interfaces at 298 K and 273 K. The average number of H-bonds is given as $\langle n_{\text{HB}} \rangle$.



Potential of Mean Force (PMF) and Microsolvation. The potential of mean force for transport of a molecule from one phase to another is one mechanism for understanding how differences in the interfacial properties impact the permeability and molecular reactions therein. In our previous work, we have discussed the free energy of solvation of pentane by water and of water by each of the pentane isomers.⁴⁶ However, the microsolvated clusters examined represented only one of many possible solvation environments that may be populated at room

temperature. The PMF study here includes an ensemble of configurations and thus is a natural extension of the DFT study.

Figure 8. A) Potential of mean force for water migration across the water:pentane interfaces and b) pentane traveling across the water:pentane interfaces in kcal/mol.



As shown in Figure S9 and 8A, water requires ~16% more energy to cross a pentane interface than to go into the vapor phase. This is in good agreement with our previous quantum mechanical studies, in which ΔG_{solv} of water by either pentane isomer was predicted to be 6-9 kcal/mol.⁴⁶ Previous work has also indicated that the water-alkane interaction is weaker near methyl groups and as such it may not be surprising that it requires slightly more energy for water to be solvated by neopentane.⁴⁶ Further, the water molecules are more organized at 273 K and thus migration into the organic phase leads to a higher loss of hydrogen bonds than at 298 K. Figure 8B represents the global PMF for transport of an *n*-pentane and neopentane molecule across their respective aqueous interfaces. Between the two pentane isomers, neopentane requires ~32% more energy to cross an aqueous interface, agreeing with the DFT prediction that aqueous solvation of neopentane is the least favorable among the two pentane isomers.⁴⁶

It is of interest to note that the umbrella sampling is fairly noisy near the phase boundary, making it difficult to ascertain the presence of a shallow minimum. Yet even if such a small minimum does exist, the kinetic features of microsolvation at the interface are likely to be the most useful for understanding differences in the interfacial properties. Thus, the explicit microsolvated species formed at the interface were studied by considering the network formed when H₂O and pentane molecules are transformed into vertices and an edge is formed when the distance between the H₂O O-atom and the pentane H-atoms is < 4.3 Å (a distance somewhat larger than the minimum in the two-body potential energy surface between those atoms).⁴⁶ Using this approach the distribution of edges about every water vertex can be turned into a representation of the number of pentane interactions and thus can be used to assess whether individual H₂O become partially or fully solvated by pentane. As observed in Figure 9A, out of all water molecules that make an edge with *n*-pentane it is most common for H₂O to interact with only a single *n*-pentane molecule (55-60% of the time). However, due to surface roughness there is an appreciable probability (up to 30%) that individual H₂O will be partially solvated by 2 - 3 *n*-pentane molecules. In prior DFT cluster based studies a “complete” solvation shell of *n*-pentane about water was found to have ~6 *n*-pentane molecules. It appears that only a small percent of H₂O (< 3%) attempt to transition into the organic phase and in doing so have 4 – 5 solvating *n*-pentane and only ~0.05% of the interfacial H₂O are ever fully solvated on the organic side of the interface. This represents 1 H₂O out of every 5600 H₂O that come in direct contact with the *n*-pentane. Interestingly, those few H₂O that do become fully microsolvated have a non-negligible persistence of 70-80 fs and are thus trapped briefly in the organic phase. Yet the most important feature of microsolvation of water is that the distributions of the

microsolvated species are nearly identical for the water:neopentane and water:*n*-pentane systems irrespective of the system temperature (Figure S10 in *Supplementary Information*).

From the perspective of *n*-pentane and the number of interactions it has with water there appears to be significant partial solvation (Figure 9B). The perpendicular arrangement of the *n*-pentane relative to the interfacial plane facilitates portions of the *n*-pentane alkyl chains to extend into the aqueous phase, causing 60% of all interfacial molecules to have 5 – 10 waters of solvation. A very broad distribution of partially solvated *n*-pentane structures is observed, however the probability of more than 10 waters of solvation about an individual *n*-pentane drops significantly with 13% of *n*-pentane molecules surrounded by 10 – 15 H₂O. In our prior work a first solvation shell of H₂O about *n*-pentane was found to have ~ 30 waters, yet even if the definition of the fully microsolvated *n*-pentane is extended to only those structures with > 20 H₂O, a mere 0.06% of all interfacial *n*-pentane fully penetrate the aqueous phase. Similar observations are made for neopentane solvated by water (Figure S10 in *Supplementary Information*). Thus microsolvation of either water in pentane or pentane in water are rare events. Yet, a significant difference in the solvation of *n*-pentane by water lies in the persistence of the microsolvated *n*-pentane clusters. These species have no significant persistence in the aqueous phase, unlike water which penetrates the organic phase and can exist there for nearly a hundred femtoseconds. The microsolvation of *n*-pentane is somewhat more temperature sensitive than the microsolvation of water, in that increased temperatures appear to enhance the number of *n*-pentane molecules that interact with 1-5 H₂O, while the remaining configurations of partially solvated clusters are fairly independent of temperature. This may be due to a slightly larger population of *n*-pentane that penetrate into the aqueous phase by only a small amount.

Specific microsolvation events of water in *n*-pentane were subsequently examined, and one observed mechanism (Figure 10) was found to involve the dynamic motion of those *n*-pentane molecules that are highly exposed to the aqueous phase, wherein their rapid migration into the *n*-pentane side of the phase boundary effectively trapped a single H₂O temporarily in the organic phase. The overall picture that emerges from these data is that though rare, microsolvated water in pentane can have an appreciable persistence in the organic phase. In contrast, microsolvated pentanes immediately move back into the pentane phase. This is likely related to the interfacial orientation of *n*-pentane, which supports partial solvation by water, yet even the methyl groups of neopentane are also surrounded by water at the interface. Unlike water, pentane molecules constantly jostle such that there is a general tendency for a portion of the molecule to be partially solvated by water – the dynamic motion of this partial solvation occasionally leads to a pentane “accidentally” being microsolvated fully by water, however the pentane immediately migrates such that it is again partially immersed in the organic phase. The motion of the pentane molecules at the interface may also be related to the microsolvation of individual H₂O in the organic phase, as the ability of the larger pentane molecules to transverse the interface may actually trap H₂O as the pentane molecules jostle in and out of being exposed to the aqueous region. Correlations between the molecular motion of the organic molecules and H₂O microsolvation is an ongoing area of research.

Figure 9. Distributions of (A) the number of *n*-pentane molecules that solvate individual H₂O, and (B) the number of water molecules that solvate individual *n*-pentane at 273 K and 298 K.

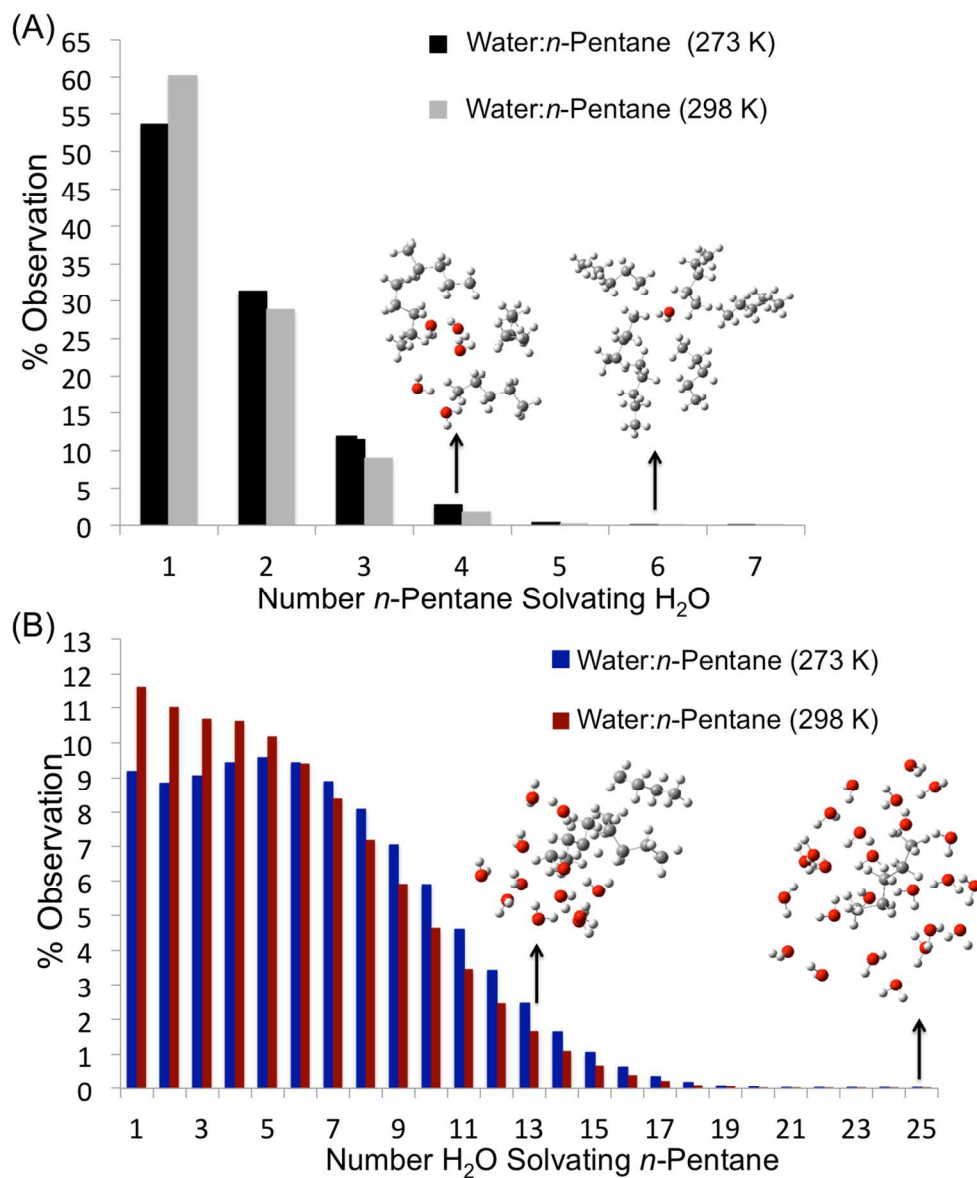
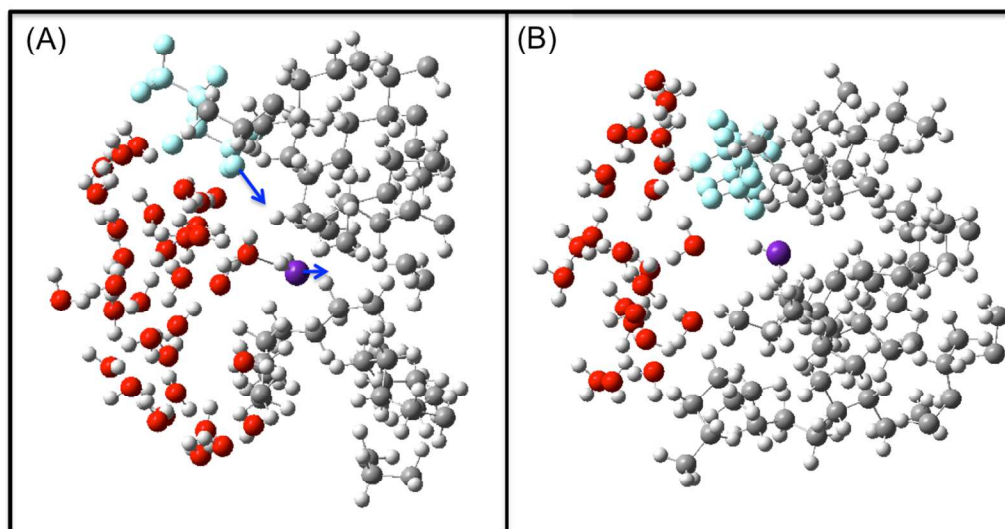


Figure 10. One observed mechanism for microsolvation of water in *n*-pentane. (A) An individual H₂O at the interface (highlighted in purple), hydrogen bonded to another water, with a nearby *n*-pentane partially solvated by interfacial water (highlighted in teal). (B) The highlighted *n*-pentane has migrated back into the organic phase, effectively trapping the highlighted H₂O in *n*-pentane.



Conclusions

The hydrogen bond network of water has been shown to respond very differently to the presence of an alkane solvent relative to a vapor interface at room temperature. Analysis of the hydrogen bond distribution of interfacial water reveals significantly more water molecules with 3- and 4- H-bonds near pentane relative to water near the vapor interface. Concurrently, the persistence of the H-bonds is also increased. As temperature is decreased both the H-bond distributions and the H-bond persistence become very similar for the vapor and pentane biphasic systems, however the hydrogen bond network properties are shown to be less temperature dependent in the presence of the pentane solvent. Overall, the trends in H-bond network

properties are less sensitive to the pentane isomer than the interfacial tension, width, molecular orientation, and density.

The largest deviations in interfacial properties arise between water:neopentane at 273 K and water:*n*-pentane at 298 K. These two systems exhibit large differences in interfacial tension and width, however close examination of both the occurrence and distribution of microsolvated species (water in pentane or pentane in water) are nearly identical. Microsolvation is a very rare event, with only 0.05% of all interfacial H₂O ever fully penetrating the pentane phase, and 0.06% of pentane molecules being completely solvated by water. However, microsolvated water in pentane can have an appreciable persistence of nearly a hundred femtoseconds, while microsolvated pentanes immediately move back into the pentane phase. This may be due to the observation that both neopentane and *n*-pentane are frequently partially solvated by water because up to half of the molecule can jut into the aqueous phase, while the other half is solvated by other pentane molecules. The ability of pentane molecules to transverse the interface and the dynamic motion of this partial solvation can lead to a pentane “accidentally” being microsolvated fully by water, however the pentane immediately migrates such that it is again partially immersed in the organic phase. The motion of the pentane molecules at the interface may be related to the microsolvation of individual water molecules in the organic phase, as the ability of the larger pentane molecules to cross the phase boundary may actually trap H₂O as the pentane molecules jostle in and out of being exposed to the aqueous phase. These observations indicate that there may be a critical difference between the mesoscale interfacial properties and molecular scale dynamic reactivity.

Acknowledgments

This work was supported by a grant from Department of Energy, Basic Energy Sciences Heavy Element program (DE-SC0001815). This research was performed using EMSL, a national scientific user facility sponsored by the Department of Energy's Office of Biological and Environmental Research and located at Pacific Northwest National Laboratory. The authors wish to thank Dr. Rene Corrales for helpful hints regarding equilibration procedures for biphasic systems and to Dr. Johannes Kästner for providing the umbrella integration sampling software program.

References

1. S. A. Patel and C. L. Brooks, *J. Chem. Phys.*, 2006, 124, 204706.
2. J. L. Rivera, C. McCabe and P. T. Cummings, *Phys. Rev. E*, 2003, 67, 011603.
3. F. Bresme, E. Chacon, P. Tarazona and K. Tay, *Phys. Rev. Lett.*, 2008, 101, 056102.
4. H. Xiao, Z. Zhen, H. Sun, X. Cao, Z. Li, X. Song, X. Cui and X. Liu, *Sci. China*, 2010, 53, 945.
5. B. A. Bauer, Y. Zhong, D. J. Meninger, J. E. Davis and S. A. Patel, *J. Mol. Graph. and Model.*, 2011, 29, 876.
6. M. L. Schlossman, *Curr. Opin. Colloid Interface Sci.*, 2002, 7, 235.
7. H. Kellay, J. Meunier and B. P. Binks, *Phys. Rev. Lett.*, 1992, 69, 1220.
8. J. Tomlinson-Phillips, J. Davis, D. Ben-Amotz, D. Spangberg, L. Pejov and K. Hermansson, *J. Phys. Chem. A*, 2011, 115, 6117.
9. G. L. Richmond, *Chem. Rev.*, 2002, 102, 2693.
10. M. G. Brown, D. S. Walker, E. A. Raymond and G. L. Richmond, *J. Phys. Chem. B*, 2003, 107, 237.
11. L. F. Scatena and G. L. Richmond, *J. Phys. Chem. B*, 2001, 105, 11240.
12. L. F. Scatena, M. G. Brown and G. L. Richmond, *Science*, 2001, 292, 908.
13. H. S. Ashbaugh, L. R. Pratt, M. E. Paulaitis, J. Clohery and T. L. Beck, *J. Am. Chem. Soc.*, 2005, 127, 2808.
14. K. Lum, D. Chandler and J. D. Weeks, *J. Phys. Chem. C*, 1999, 103, 4570.
15. F. H. Stillinger, *J. Solution Chem.*, 1973, 2, 141.
16. D. M. Mitrinovic, A. M. Tikhonov, M. Li, Z. Q. Huang and M. L. Schlossman, *Phys. Rev. Lett.*, 2000, 85, 582.
17. D. M. Mitrinovic, Z. Zhang, S. M. Williams, Z. Huang and M. L. Schlossman, *J. Phys. Chem. B*, 1999, 103, 1779.
18. A. Zorbakhsh, J. Bowers and J. Webster, *Meas. Sci. Technol.*, 1999, 10, 738.
19. J. Bowers, A. Zorbakhsh, J. Webster, L. Hutchings and R. Richards, *Langmuir*, 2001, 17, 140.
20. A. Braslau, M. Deutsch, P. S. Pershan, A. H. Weiss, J. Als-Nielsen and J. Bohr, *Phys. Rev. Lett.*, 1985, 54, 114.
21. I. Benjamin, *Annu. Rev. Phys. Chem.*, 1997, 48, 407.
22. A. E. Ismail, G. S. Grest and M. J. Stevens, *J. Chem. Phys.*, 2006, 125, 014702.
23. X. G. Ye, S. T. Cui, V. F. de Almeida and B. Khomami, *J. Phys. Chem. B*, 2013, 117, 14835.
24. A. R. Vanbuuren, S. J. Marrink and H. J. C. Berendsen, *J. Phys. Chem.*, 1993, 97, 9206.
25. W. Gan, D. Wu, Z. Zhang, Y. Guo and H. F. Wang, *Chin. J. Chem. Phys.*, 2006, 19, 20.
26. J. Chang and S. I. Sandler, *J. Chem. Phys.*, 2004, 121, 7474.
27. D. J. Price and C. L. Brooks, *J. Chem. Phys.*, 2004, 121, 10096.
28. S. Plimpton, A. Thompson, P. Crozier and L. M. D. Simulator, LAMMPS Molecular Dynamics Simulator <http://lammps.sandia.gov>.
29. L. Martínez, R. Andrade, E. G. Birgin and J. M. Martínez, *J. Comp. Chem.*, 2009, 30, 2157.
30. W. G. Hoover, *Phys. Rev. A*, 1985, 31, 1695.
31. S. Nose, *J. Chem. Phys.*, 1984, 81, 511.
32. J. M. Thijssen, *Computational Physics*, Cambridge University Press, 2007.
33. M. D. Lacasse, G. S. Grest and A. J. Levine, *Phys. Rev. Lett.*, 1998, 80, 309.

34. T. Schneider and E. Stoll, *Phys. Rev. B*, 1978, 17, 1302.
35. I. Rips, J. Klafter and J. Jortner, *J. Chem. Phys.*, 1988, 88, 3246.
36. C. D. Wick and L. X. Dang, *J. Phys. Chem. B*, 2005, 109, 15574.
37. F. P. Buff, R. A. Lovett and F. H. Stillinger, *Phys. Rev. Lett.*, 1965, 15, 621.
38. J. S. Huang and W. W. Webb, *J. Chem. Phys.*, 1969, 50, 3677.
39. D. Beysens and M. Robert, *J. Chem. Phys.*, 1987, 87, 3056.
40. S. Senapati and M. L. Berkowitz, *Phys. Rev. Lett.*, 2001, 87, 176101.
41. S. W. Sides, G. S. Grest and M.D. Lacasse, *Phys. Rev. E* 60, 1999, 60, 6708.
42. J. Rowlinson and B. Widom, *Molecular Theory of Capillarity*, Clarendon Press, Oxford, 1982.
43. A. Ozkanlar and A. E. Clark, *J. Com. Chem.*, 2014, 35, 495.
44. A. N. Semenov, *Macromolecules*, 1994, 27, 2732.
45. H. S. Ashbaugh, L. R. Pratt, M. E. Paulaitis, J. Clohery and T. L. Beck, *J. Am. Chem. Soc.*, 2005, 127, 2808.
46. Y. Ghadar and A. E. Clark, *J. Chem. Phys.*, 2012, 136, 054305.
47. G. M. Torrie and J.P.Valleau, *J. Com. Phys.*, 1977, 23, 187.
48. J. Kästner and W. Thiel, *J. Chem. Phys.*, 2005, 123, 144104.
49. J. Kästner and W. Thiel, *J. Chem. Phys.*, 2006, 124, 234106.
50. J. Kästner, *Comp. Mol. Sci.*, 2011, 1, 932.
51. H. W. Horn, W. C. Swope, J. W. Pitera, J. D. Madura, T. J. Dick, G. L. Hura and T. Head-Gordon, *J. Chem. Phys.*, 2004, 120, 9665.
52. S. K. Lee and S. H. Lee, *Bull. Korean Chem. Soc.*, 1999, 20, 897.
53. S. H. Lee, H. Lee and H. Pak, *Bull. Korean Chem. Soc.*, 1997, 18, 478.
54. Z. Bochynski and H. Drozdowski, *Phys. Chem. Liq.*, 2001, 39, 189.
55. S. H. Lee, H. Lee, H. Pak and J. C. Rsaiah, *Bull. Korean Chem. Soc.*, 1996, 17, 735.
56. F. W. Starr, J. K. Nielsen and H. E. Stanley, *Phys. Rev. E*, 2000, 26, 579.
57. D. Chakraborty and A. Chandra, *J. Chem. Phys.*, 2011, 135, 114510.
58. R. S. Taylor, L. X. Dang and B. C. Garrett, *J. Phys. Chem.*, 1996, 100(28), 11720.
59. I. M. Svishchev and P. G. Kusalik, *J. Chem. Soc. Farad. Trans.*, 1994, 90, 1405.
60. F. N. Keutsch, R. S. Fellers, M. G. Brown, M. R. Viant, P. B. Petersen and R. J. Saykally, *J. Am. Chem. Soc.*, 2001, 123, 5938.
61. M. Praprotnik, D. Janezic and J. Mavri, *J. Phys. Chem. A*, 2004, 108, 11056.
62. M. P. Allen and D. J. Tildesley, *Computer Simulations of Liquids*, Oxford Science, Oxford, 1987.
63. L. X. Dang and T. M. Chang, *J. Chem. Phys.*, 1997, 19, 106.
64. R. Sakamaki, A. K. Sum, T. Narumi and K. Yasuoka, *J. Chem. Phys.*, 2011, 134, 124708.
65. C. Vega, E. Sanz and J. L. F. Abascal, *J. Chem. Phys.*, 2005, 122, 114507.
66. J. G. Harris, *J. Phys. Chem.*, 1992, 96(12), 5077.
67. A. P. Froba, L. P. Pellegrino and A. Leipertz, *Int. J. Thermophys.*, 2004, 25, 1323.
68. M. Mohsen-Nia, H. Rasa and S. F. Naghibi, *J. Chem. Thermodyn.*, 2010, 42, 110.
69. J. J. Jasper, *J. Phys. Chem. Ref. Data*, 1972, 1, 841.
70. F. Goujon, P. Malfrey, J.-M. Simon, A. Boutin, B. Rousseau and A. H. Fuchs, *Mol. Sim.*, 2001, 27, 99.
71. A. Goebel and K. Lunkenheimer, *Langmuir*, 1997, 13, 369.
72. H. Kahl, T. Wadewitz and J. Winkelmann, *J. Chem. Eng. Data*, 2003, 48, 580.

73. F. Goujon, P. Malfreyt, J.-M. Simon, A. Boutin, B. Rousseau and A. H. Fuchs, *J. Chem. Phys.*, 2004, 121, 12559.
74. Z. Hu and J. D. Weeks *J. Phys. Chem. C*, 2010, 114, 10202.
75. S. Zeppieri, J. Rodriguez and A. d. Ramol, *J. Chem. Eng. Data*, 2001, 46, 1086.
76. T. Chang and L. X. Dang, *J. Chem. Phys.*, 1996, 104, 6772.